# Open-circuit voltage decay: moving to a flexible method of characterisation

Antoine Lemaire, Arnaud Perona, Matthieu Caussanel, Hervé Duval, Alain Dollet

*IET Circuits, Devices & Systems*

# Open-Circuit Voltage Decay: Moving to a Flexible Method of Characterization

*A. Lemaire*[1,2], *A. Perona*[1,2*], *M. Caussanel*[1,2], , *H. Duval*[1,2], , *A. Dollet*[2]

[1] *Universty of Perpignan Via Domitia (UPVD), 52 avenue Paul Alduy, 66100, Perpignan, France*
[2] *PROcesses, Materials and Solar Energy laboratory (PROMES-CNRS), Rambla de la thermodynamique, 66100, Perpignan, France*
* *E-mail: arnaud.perona@univ-perp.fr*

**Abstract:** Open-Circuit Voltage Decay is a method to characterize minority carrier effective lifetime ($\tau_{eff}$). It is non-destructive, simple and low-cost. It has been mainly used in silicon p-n junctions. $\tau_{eff}$ is a very important parameter to optimize device design but also to supervise process steps. Actually, it is not the only parameter we can obtain by OCVD. Due to the intrinsic space charge region (SCR) capacitance of a p-n junction, doping level of the lowest-doped region ($N_l$) and built-in potential ($V_{bi}$) are extractable. Moreover, it is also possible to obtain the shunt resistance ($R_{sh}$) value when it has a significant effect on the p-n junction behaviour. We first applied the well-established one-diode model in transient regime to simulate OCVD signal. In a second step, we used an optimization algorithm to fit the experimental curve of a silicon diode in order to extract $\tau_{eff}$, $N_l$, $V_{bi}$ and $R_{sh}$. These values were compared to those obtained from C-V and I-V. Results are promising and demonstrates for the first time, the flexibility of the OCVD method. It opens up the perspective for development of add-on features of the method and for measuring short lifetime.

## 1 Introduction

Minority carrier lifetime measurement is of major importance to optimize electronic and optoelectronic devices such as solar cells [1]. It enables to tailor solar cells characteristics such as bulk thickness and doping levels. Moreover, when lifetime can be measured between process steps, it also gives a follow-up of these various steps quality. Indeed, lifetime depends on material nature and on the various treatments the material or device have been subjected to [2]. That's why it informs on material purity combined with interface quality. Measured lifetime always results from several electrons-holes recombination mechanisms such as SRH (Shockley-Read-Hall), Auger and radiative [3] and thus is called effective lifetime $\tau_{eff}$.

Nowadays, photoconductance decay (PCD) [4, 5] is commonly used for silicon solar cells. It is a contactless method which allows really fast characterization. However, the method expects equipments (light flash and filter) specific to the characterized semiconductor and does not allow to measure short lifetimes ($< 1\,\mu s$). Time-resolved photoluminescence (TRPL) [6] allows lifetime measurement down to the ps scale. It is usually applied to III-V and II-IV semiconductors for that reason. This method is usually slow when applied to materials having poor quality and/or bad radiative properties. Furthermore, it is an expensive method compared to PCD.

By comparison, Open-Circuit Voltage Decay (OCVD) is fast, low-cost (as the PCD) and enables characterization of COTS devices. Moreover, it allows characterization of any semiconductors, no matter its band gap: wide/narrow and direct/indirect. However, due to several drawbacks it has been scarcely employed to measure short lifetime. It requires electrical contacts plus a junction (p-n or Schottky) and its signal is often blurred by the space charge region (SCR) effects (capacitive and generations/recombinations (G/R) current) [7]. These effects make the method rather subjective for measuring $\tau_{eff}$. A well-known method, the "Suns-$V_{oc}$" [8], has been developed on the basis of the QSS-PCD [5] to avoid SCR capacitive effect. However, the bulk doping level of the junction must be known.

Our approach is to take advantage of capacitive effect and to the best of our knowledge, this has never been investigated. The SCR capacitance of an asymmetric junction (n-$p^+$ or p-$n^+$) depends on the doping level of the lowest-doped region and built-in voltage, whereas SCR G/R current can be first approximated to a simple shunt resistance. The flexibility of the OCVD makes it extremely attractive since none of the methods faced here can compete. Thus, according to theory these quantities can be extracted by assuming a proper fitting model. Therefore, this is the purpose of this paper.

## 2 OCVD Theory

OCVD theory was initially exposed in 1955 by Gossick [9] and Lederhandler & Giacoletto [10]. It has been first developed to characterize germanium (Ge) but it was quickly applied to silicon (Si). In theory, it is suitable to any semiconductors. Its working principle is based on the interpretation of the open-circuit voltage decay across a junction after an excitation pulse. First, the junction is forward biased either electrically or optically [11]. Then, open-circuit condition is provided by a pulse generator or by a switch like a MOSFET. Finally, the voltage decay across the open-circuited junction is recorded over the time. There are two types of circuits using a switch: the so-called series circuit where switch and characterized junction are in series [12–15] (voltage bias source) and the so-called parallel where they are in parallel [15–17] (current bias source). The simplicity of the circuit makes the method low-cost and easy to operate. Usually, OCVD signal exhibits 3 regions (see Fig. 1).

Region (i) is an abrupt voltage drop mainly due to series resistance [12].

Region (ii) is due to diffusion/recombination of minority charge carriers into quasi neutral regions (QNR). This is the region of interest for lifetime extraction. Ideally, region (ii) presents a linear decay whose slope is inversely proportional to effective lifetime $\tau_{eff}$:

$$\tau_{eff} = -\frac{\eta k_B T}{q} \frac{1}{\mathrm{d}V/\mathrm{d}t} \tag{1}$$

where $\eta$ is the p-n junction ideality factor, $k_B$ the Boltzmann constant in $\mathrm{J\,K^{-1}}$, $T$ the temperature in K, $q$ the elementary electric charge in C and $\mathrm{d}V/\mathrm{d}t$ the voltage decay rate in $\mathrm{V\,s^{-1}}$. $\eta$ depends on injection level and dominant recombination mechanism [18]. This linear behaviour eases greatly $\tau_{eff}$ extraction and makes the method really simple in terms of analysis. However, the linear OCVD decay has an intrinsic limit, depending on materials [15]. Indeed, for short lifetimes or highly-doped junctions, there isn't region (ii) any more [15]. Furthermore, for intermediate lifetimes or doping levels, the method becomes rather subjective because it depends on where you clearly identify the linear region.

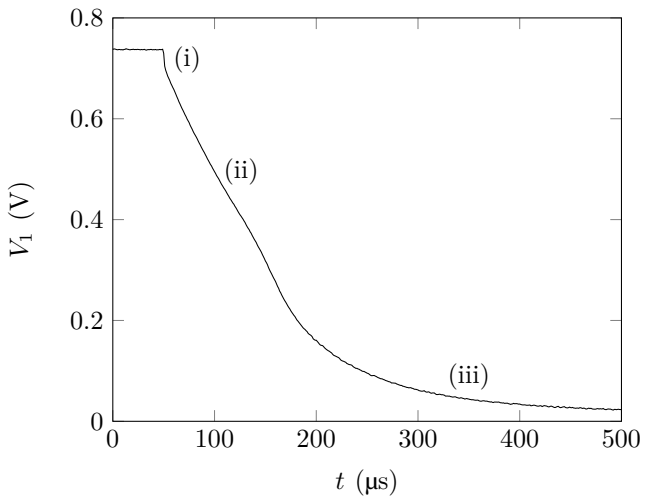


**Fig. 1**: Typical OCVD signal of a silicon diode under moderate injection obtained by "series circuit".

In transient regime, minority charge carriers stored into QNRs behave like a capacitance. This diffusion capacitance [19] (in $\mathrm{F\,cm^{-2}}$) is defined by:

$$C_D = \frac{q}{\eta k_B T}\tau_{eff} J(V) \tag{2}$$

where $J(V)$ is the current density of the p-n junction in $\mathrm{A\,cm^{-2}}$ derived from the Shockley equation.

Region (iii) is due to SCR capacitance which typically decreases decay rate [7]. Experimentally, it makes region (ii) usually tough to identify and thus unreliable. Moreover, the lower the lifetime, the more difficult the region (ii) identification. SCR capacitance depends on material and junction design (doping levels) and is defined [18] according to the following formula:

$$C_{SCR} = \frac{\epsilon}{W_{SCR}} = \sqrt{\frac{q\epsilon N_A N_D}{2(N_A + N_D)(V_{bi} - V)}} \tag{3}$$

where $C_{SCR}$ is the SCR capacitance in $\mathrm{F\,cm^{-2}}$, $\epsilon$ the semiconductor permittivity in $\mathrm{F\,cm^{-1}}$, $W_{SCR}$ the thickness of the SCR in cm, $N_A$ ($N_D$) the acceptors (donors) doping level of the p-doped (n-doped) QNR in $\mathrm{cm^{-3}}$, $V_{bi}$ the built-in potential in V and $V$ the voltage across the SCR in V. $V_{bi}$ is calculated [18] through:

$$V_{bi} = \frac{k_B T}{q} \ln\left(\frac{N_A N_D}{n_i^2}\right) \tag{4}$$

where $n_i$ is the intrinsic carriers density in $\mathrm{cm^{-3}}$. When a p-n junction is asymmetric (n-p$^+$ or p-n$^+$), (3) may be written in the following form:

$$C_{SCR} = \sqrt{\frac{q\epsilon N_l}{2(V_{bi} - V)}} \tag{5}$$

where $N_l$ is the doping level of the lowest-doped QNR in $\mathrm{cm^{-3}}$. SCR capacitance actually acts in parallel with diffusion capacitance, thus global capacitance is always the sum of them. Nevertheless, for a voltage higher than $V_{bi}$, SCR region and its capacitance disappear. In this case, OCVD signal is fully due to diffusion capacitance. As the voltage across the diode decreases over the time, the inner electric field $E_i$ and SCR capacitance reappear. Then, SCR capacitance decreases OCVD decay rate when its value becomes higher than diffusion capacitance. SCR capacitance makes decay rate lower because $E_i$ induces a strong increase of instantaneous resistance [11]. However, decay rate after region (ii) can also be increased with low shunt resistance [7]. Shunt resistance effect is often attributed to G/R into the SCR [7] and perimeter recombinations in case of small area samples like solar cells dedicated to CPV [20, 21]. Therefore region (iii) is filled with information.

For a given material, (5) clearly shows that SCR capacitance depends on $N_l$, $V_{bi}$ and $V$. However, to the best of our knowledge, region (iii) has never been exploited as it could be. Thus, applying a fitting model to OCVD measurements theoretically allows to extract $N_l$ and $V_{bi}$. Shunt resistance $R_{sh}$ is also extractable when it has a strong influence on OCVD signal. In addition, being able to fit the entire signal allows more objective and accurate lifetime determination when region (ii) identification is difficult.

## 3 Modelling

OCVD signal modelling was carried out with Python programming language [22] which provides many powerful libraries that allow data treatment, numerical computation, optimization and so on. Moreover it works on almost all operating systems (Windows, Linux/UNIX, Mac OS X and so on). We used Python 3.7.1 with Anaconda 4.2.0 distribution on Spyder environment. We developed a model and first compared it to *Mahan and Barnes (M&B)* previous work [7]. Then we studied the influence of several parameters such as $\tau_{eff}$, $N_l$, $V_{bi}$ and $R_{sh}$ on OCVD signal.

### *3.1 One-diode model*

The model we developed is based on the lumped element model of one asymmetric diode in transient regime [23] which is represented Fig. 2. Our work has been inspired by *M&B* one's [7] who simulated OCVD

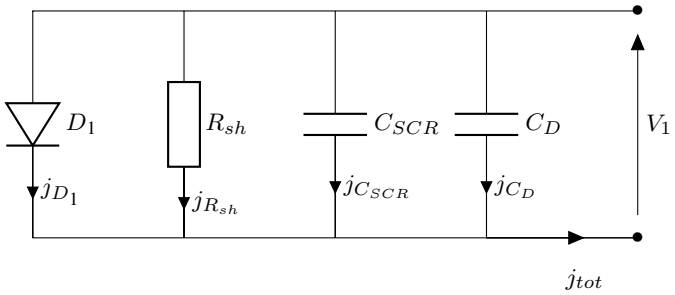


**Fig. 2**: Lumped element model of one asymmetric diode in transient regime.

signal in 1981. They used two different models: a one-diode model to simulate SCR capacitance effect and a two-diode model to simulate effect of the G/R current into the SCR. The second diode from the model #2 is similar to a shunt resistance having a dynamic behaviour. In our model, the G/R current into the SCR was assigned to a constant resistance so-called shunt resistance. In first approximation, this has no major influence on the global behaviour because the G/R current into the SCR is known to occur at low voltage over a short range. However we applied a dynamic behaviour (voltage dependence) to the SCR capacitance while *M&B* considered a constant one.

Moreover, we simulated influences of SCR capacitance and leakage current into the SCR together whereas they did it separately: at least they didn't show influence when both have significant effects. Therefore, they didn't show their mutual influence. Unfortunately, we didn't take into account the series resistance because it requires a current flowing at $t = 0$, so it does not fulfil the open-circuit condition. Details of the models and their differences are summarized in the Table 1.

The lumped element model of OCVD represented in Fig. 2 leads to the following equation expressing the total current density in

**Table 1** Comparison between *M&B* models [7] and ours.

| | *M&B* #1 | *M&B* #2 | Lemaire et al. |
|---|---|---|---|
| Assignement of $C_{SCR}$ effect | Capacitance (constant) | $\asymp$ | Capacitance (voltage-dependent) |
| Assignement of G/R current effect | $\asymp$ | Diode (voltage-dependent) | Resistance (constant) |
| Model | one-diode | two-diode | one-diode |

$\mathrm{A\,cm^{-2}}$:

$$J_{tot} = J_{D1} + J_{Rsh} + J_{C_{SCR}} + J_{C_D} \tag{6}$$

where $J_{D1}$, $J_{Rsh}$, $J_{C_{SCR}}$ et $J_{C_D}$ are the current densities through diode D1, shunt resistance $R_{sh}$, SCR capacitance $C_{SCR}$ and diffusion capacitance $C_D$ respectively. $J_{D1}$ corresponds to the Shockley equation mentionned in (2). Diffusion capacitance in an n-p$^+$ (p-n$^+$) junction deals with hole diffusion (electron diffusion) into the n-doped (p-doped) QNR. By expressing all these current densities in a p-n$^+$ junction, we can rewrite (6) as:

$$J_{tot} = \frac{Q_n(t)}{\tau_n} + \frac{V_1(t)}{R_{sh}} + C_{SCR}(t)\frac{dV_1(t)}{dt} + \frac{dQ_n(t)}{dt} \tag{7}$$

with:

$$Q_n(t) = Q_{n0}\left[\exp\left(\frac{V_1(t)}{\eta V_{th}}\right) - 1\right] \tag{8}$$

$$Q_{n0} = q\frac{n_i^2}{N_A}\sqrt{D_n\tau_n} \tag{9}$$

where $Q_n$ is the electron density into p-doped QNR in $\mathrm{C\,cm^{-2}}$, $Q_{n0}$ the electron density into p-doped QNR at thermal equilibrium in $\mathrm{C\,cm^{-2}}$, $\tau_n$ the electron lifetime in s, $V_1$ the OCVD voltage in V, $R_{sh}$ the shunt resistance in $\Omega\,\mathrm{cm^2}$ and $C_{SCR}$ the SCR capacitance in $\mathrm{F\,cm^{-2}}$. $N_A$ is the acceptor doping level. It corresponds also to the doping level of the lowest-doped region, so $N_A = N_l$. As the p-n junction is asymmetric we assumed $\tau_n$ is equal to $\tau_{eff}$ [7]. During OCVD measurement, it is assumed that $J_{tot} = 0$ because of the open-circuit condition. Then, simulation of the $V_1$ decay is performed by solving the following 1$^{\text{st}}$ order ordinary differential equation (ODE):

$$0 = \frac{Q_{n0}}{\tau_n}\left[\exp\left(\frac{V_1(t)}{\eta V_{th}}\right) - 1\right] + \frac{V_1(t)}{R_{sh}} + \frac{dV_1(t)}{dt}\left[\frac{Q_{n0}}{\eta V_{th}}\exp\left(\frac{V_1(t)}{\eta V_{th}}\right) + C_{SCR}(t)\right] \tag{10}$$

We used the function "odeint" [24] provided by Python-SciPy library called "scipy.integrate" to solve the ODE. The resolution method is Adams/BDF [25].

### 3.2 Comparison to Mahan and Barnes (M&B) model

First modelling results have been obtained using *M&B* parameters [7]. They are presented in the following Table:

**Table 2** Parameters of *M&B* models [7] at 300 K.

| $D$ [$\mathrm{cm^2\,V^{-1}\,s^{-1}}$] | $N_l$ [$\mathrm{cm^{-3}}$] | $n_i$ [$\mathrm{cm^{-3}}$] | $\epsilon_r$ [-] | $V_{bi}$ [V] | $\tau_{eff}$ [µs] |
|---|---|---|---|---|---|
| 20 | $1\times10^{16}$ | $1\times10^{10}$ | 11.8 | 0.93 | 1 |

Fig. 3 shows four different OCVD signals. First, we note that there is no region (i) because no series resistance has been taken into account. The curve without (w/o) shunt resistance represents OCVD signal without major leakage current into the SCR and so the signal is solely governed by diffusion and SCR capacitances. $C_{SCR}$ decreases decay rate into region (iii). On the other hand, the signal increases it abruptly without major SCR capacitance effects but with major leakage current into the SCR. When SCR capacitance and shunt resistance are omitted, the signal is only due to diffusion capacitance and it is linear over the entire decay. Therefore, region (iii) is logically vanished. OCVD decay without diffusion capacitance represents the case when lifetime is so small that region (ii) is completely fused with region (iii) [15]. These results are consistent regarding the theory and similar to those obtained by [7].

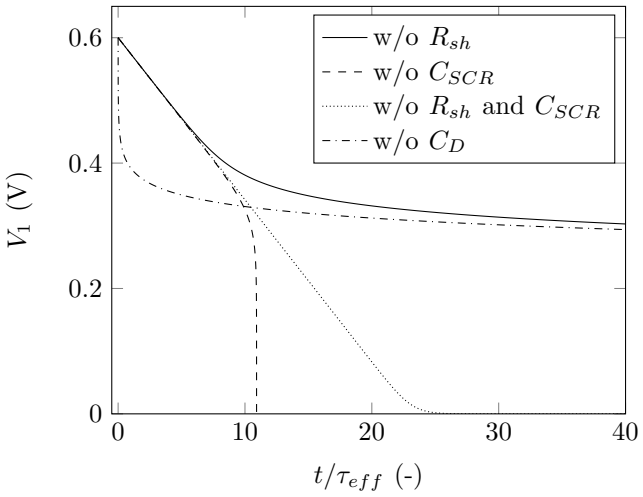


**Fig. 3**: OCVD signals simulated according to *M&B* parameters [7].

As we previously explained, the work of *M&B* didn't consider the dynamics of SCR capacitance. Then, we compared our model to their one-diode model with two different applied voltages $V_a$ (0.9 V and 0.6 V) below the built-in voltage $V_{bi}$ (0.93 V) in Fig. 4. For the model of *M&B*, we calculated the SCR capacitance at $V_a$. Results shows

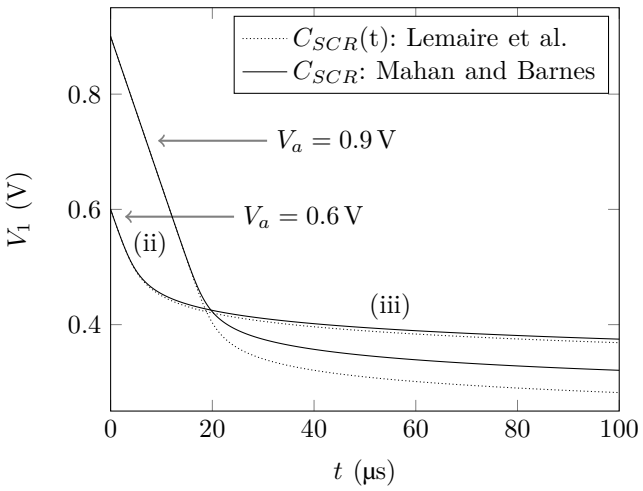


**Fig. 4**: Comparison of OCVD signals simulated with constant SCR capacitance (*M&B* model [7]) and voltage-dependent SCR capacitance (Lemaire *et al.* model).

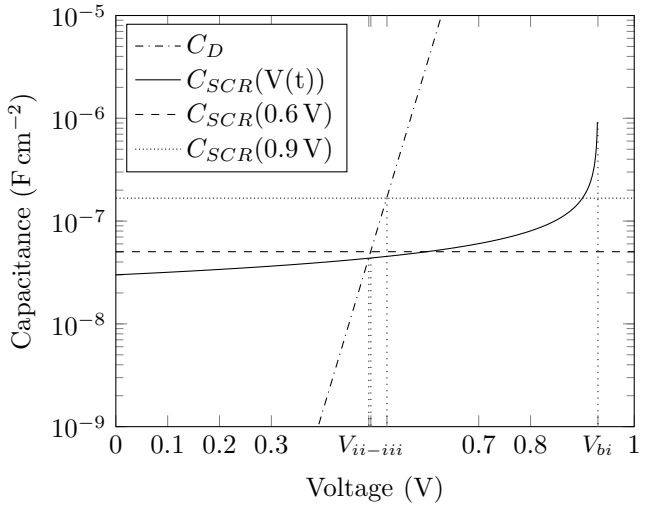


**Fig. 5**: Diffusion and SCR capacitances over the voltage according to *M&B* parameters [7].

varying influences on region (iii) depending on $V_a$. The dynamics of SCR capacitance has a greater influence when $V_a$ is higher. Indeed, the closer $V_a$ from $V_{bi}$, the higher the SCR capacitance. This is clearly shown in Fig. 5 where diffusion and SCR capacitance evolutions over the voltage are presented.

$V_{ii-iii}$ represented in Fig. 5 is the voltage for which SCR capacitance is equal to diffusion capacitance. It can be seen as the transition voltage between region (ii) and region (iii). The lower the voltage, the lower the slope of the voltage-dependent SCR capacitance $C_{SCR}(V(t))$. Its most important variation occurs around the built-in voltage that is, when SCR is really thin.

The difference appearing Fig. 4 in region (iii) is the motivation for taking the dynamics of SCR capacitance into account since we wanted to extract accurately $N_l$, $V_{bi}$ and $R_{sh}$ from this region.

### 3.3 Parametric study

This study allows to better understand OCVD behaviour. We studied the influences of the effective lifetime ($\tau_{eff}$), doping level of the lowest-doped region ($N_l$), shunt resistance ($R_{sh}$) and built-in voltage ($V_{bi}$) on the OCVD signal of a silicon p-n$^+$ junction. The default parameters of the model are reported in Table 3. $N_h$ is the doping

**Table 3** Default parameters of silicon at 300 K and for $V_a = 0.8$ V.

| $N_l$ [cm$^{-3}$] | $N_h$ [cm$^{-3}$] | $n_i$ [cm$^{-3}$] | $\epsilon_r$ [-] | $R_{sh}$ [$\Omega$ cm$^2$] | $\tau_{eff}$ [µs] |
|---|---|---|---|---|---|
| $1 \times 10^{15}$ | $1 \times 10^{19}$ | $1 \times 10^{10}$ | 11.7 | $1 \times 10^{19}$ | 1 |

level of the highest-doped region and $\epsilon_r$ the relative electrical permittivity of silicon. All simulations were performed for a p-n$^+$ junction with a ratio $N_h/N_l > 100$. The built-in voltage $V_{bi}$ was calculated from (4) and shunt resistance was overestimated on purpose to omit its influence. The diffusion coefficient $D_n$ was calculated through electron mobility $\mu_n$ in cm$^2$ V$^{-1}$ s$^{-1}$ using the following equation:

$$D_n = \frac{k_b T}{q} \mu_n \tag{11}$$

Electrons mobility was calculated according to the doping-dependent model of Masetti [26] expressed here:

$$\mu_M = \mu_1 \exp\left(\frac{-P_c}{N}\right) + \frac{\mu_c - \mu_2}{1 + \left(\frac{N}{C_r}\right)^{\alpha}} - \frac{\mu_3}{1 + \left(\frac{C_s}{N}\right)^{\beta}} \tag{12}$$

The parameters for (12) are provided Table 4.

**Table 4** Parameters of Masetti mobility model in silicon at 300 K [26].

| | electrons | holes |
|---|---|---|
| $\mu_c$ [cm$^2$ V$^{-1}$ s$^{-1}$] | 1417 | 470.5 |
| $\mu_1$ [cm$^2$ V$^{-1}$ s$^{-1}$] | 52.2 | 44.9 |
| $\mu_2$ [cm$^2$ V$^{-1}$ s$^{-1}$] | 52.2 | 0 |
| $\mu_3$ [cm$^2$ V$^{-1}$ s$^{-1}$] | 43.4 | 29 |
| $P_c$ [cm$^{-3}$] | 0 | $9.23 \times 10^{16}$ |
| $C_r$ [cm$^{-3}$] | $9.68 \times 10^{16}$ | $2.23 \times 10^{17}$ |
| $C_s$ [cm$^{-3}$] | $3.43 \times 10^{20}$ | $6.1 \times 10^{20}$ |
| $\alpha$ [-] | 0.68 | 0.719 |
| $\beta$ [-] | 2 | 2 |

#### 3.3.1 Lifetime:

Simulated OCVD signal for the various lifetimes $\tau_{eff}$ is presented in Fig. 6. We normalized x axis by $\tau_{eff}$ in order to plot all the results on the same figure. We know from (7) and (2) that diode current and diffusion capacitance are lifetime dependent. Thus, the slope of region (ii) would be as low as the lifetime is high according to (1). Because of the x axis normalization, the three slopes are the same. On the other hand, the most important influence is related to $V_{ii-iii}$: the lower the lifetime, the higher $V_{ii-iii}$. Thus for lower lifetime, duration of region (ii) is reduced for a given doping level $N_l$ and a given applied voltage $V_a$. This can be explained by the reduction of diffusion capacitance with lower lifetime (2). If the diffusion capacitance is lower, the SCR capacitance influence appears at higher voltage and so earlier, reducing region (ii) duration. It means that the lifetime extraction accuracy is reduced with decreasing lifetime.

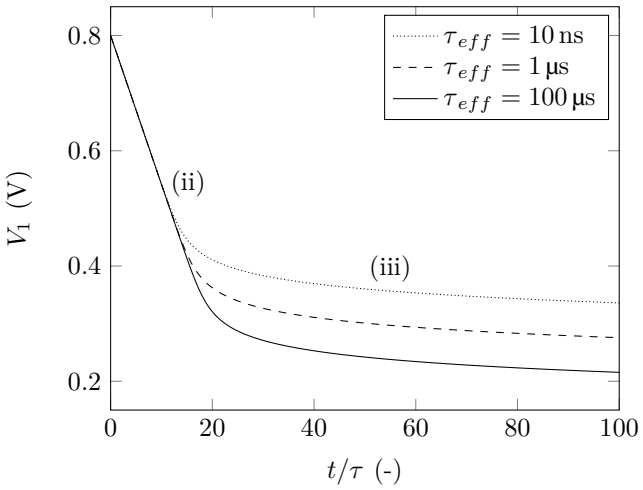


**Fig. 6**: Simulated OCVD signals for various lifetimes $\tau_{eff}$

#### 3.3.2 Doping level of the lowest-doped region:

Fig. 7 represents simulated OCVD signals for several doping levels $N_l$. We observe that $V_{ii-iii}$ increases either with increasing $N_l$ or with decreasing $\tau_{eff}$ as we saw previously. According to (5) and (2), $N_l$ which represents majority carriers density, influences both capacitances (diffusion and SCR). Increasing $N_l$ reduces the minority carriers density (i.e. decreases the diffusion capacitance) with a dependence to $1/N_l$ on the one hand, and reduces the SCR thickness (i.e. increases the SCR capacitance) with a dependence to $\sqrt{N_l}$ on the other hand. These double and imbalanced influences makes the effect of $N_l$ stronger on the signal, than its of $\tau_{eff}$. Indeed, a change of $\tau_{eff}$ by two orders of magnitude has less influence than one oder of magnitude of $N_l$. Therefore, the lifetime extraction accuracy is also reduced as well with increasing $N_l$ since this reduces the region (ii) duration.

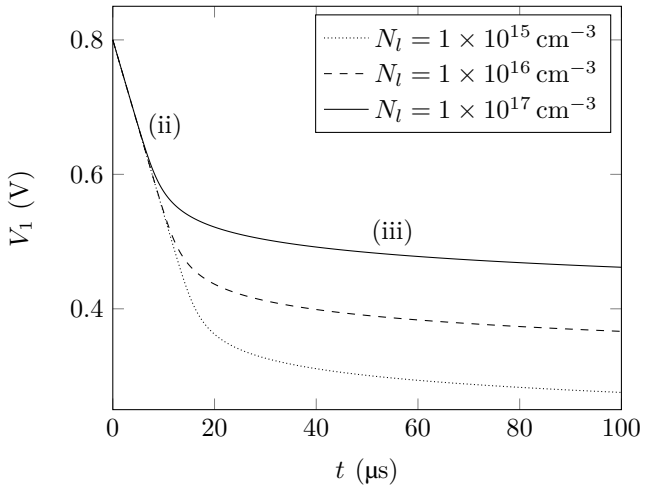


**Fig. 7**: Simulated OCVD signals for various doping levels $N_l$

### 3.3.3 *Shunt resistance:*

To the best of our knowledge, the effect of the shunt resistance on the OCVD signal has never been investigated jointly with the presence of a SCR capacitance. This investigation has been conducted here thanks to modelling (see Fig. 8). First, as *M&B* have previously demonstrated [7], we observe that $V_1$ decay rate increases with decreasing shunt resistance, i.e. with increasing leakage current. Indeed, shunt resistance is a bypass for charge carriers stored into QNR (diffusion capacitance) and SCR which makes recombinations faster (see Fig. 8). OCVD signal for $R_{sh} = 1 \times 10^{19}\,\Omega\,\mathrm{cm}^2$ can be considered free from shunt resistance influence because of its high value. However, region (iii) is influenced for $R_{sh} = 1 \times 10^{4}\,\Omega\,\mathrm{cm}^2$. On the other hand, region (ii) and region (iii) are both affected for $R_{sh} = 1 \times 10^{2}\,\Omega\,\mathrm{cm}^2$ and $R_{sh} = 1 \times 10^{3}\,\Omega\,\mathrm{cm}^2$. Indeed, the shunt resistance decrease and the SCR capacitance increase, have opposite influences on the OCVD signal. Thus region (ii) can also be affected as soon as the diode instantaneous resistance is roughly equal to the shunt resistance. Therefore, its duration may be extended when both effects balance each other. This is shown in Fig. 8 for $R_{sh} = 1 \times 10^{3}\,\Omega\,\mathrm{cm}^2$. In this specific case, the lifetime extraction accuracy is enhanced. This is precisely from that phenomenon that *Green* has created his alternative circuit [12]. He wanted to increase the accuracy of region (ii) identification by cleverly playing with these antagonistic effects. But this required to find a suitable configuration for each characterized samples. Finally, when the shunt resistance has a strong influence ($R_{sh} = 1 \times 10^{2}\,\Omega\,\mathrm{cm}^2$), $V_{ii-iii}$ is shifted up and the lifetime extraction accuracy is reduced.

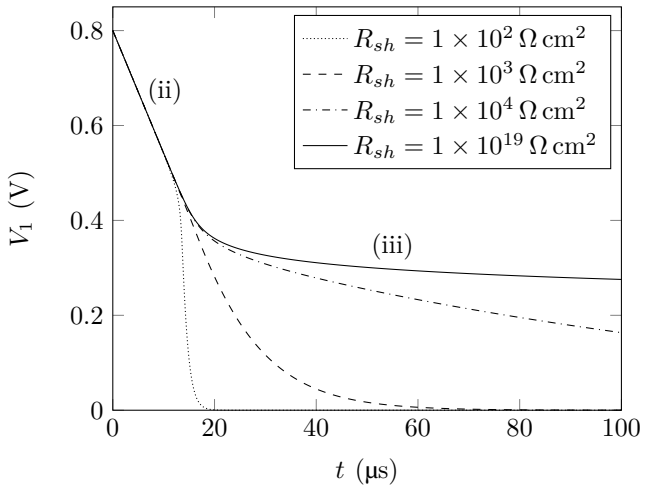


**Fig. 8**: Simulated OCVD signals for various shunt resistances $R_{sh}$

### 3.3.4 *Built-in voltage:*

The built-in voltage $V_{bi}$ depends on $N_l$ and $N_h$ for a given material according to (4). Therefore, we varied $N_h$ from $3.4 \times 10^{18}\,\mathrm{cm}^{-3}$ to $1.1 \times 10^{20}\,\mathrm{cm}^{-3}$ in order to change $V_{bi}$ (from 0.805 V to 0.894 V) but we kept $N_l = 1 \times 10^{15}\,\mathrm{cm}^{-3}$ in order to work with an asymmetric p-n junction where $N_h/N_l > 1000$. The variation of $V_{bi}$ does not significantly affect the OCVD signal (see Fig. 9). $V_{bi}$ defines the value of the voltage below which a SCR capacitance appears. However, since the diffusion capacitance is much higher than the SCR capacitance for this particular value of the lifetime, its influence remains negligible. It means that $V_{bi}$ extraction from region (iii) would be rather complicated if diffusion capacitance is too high.

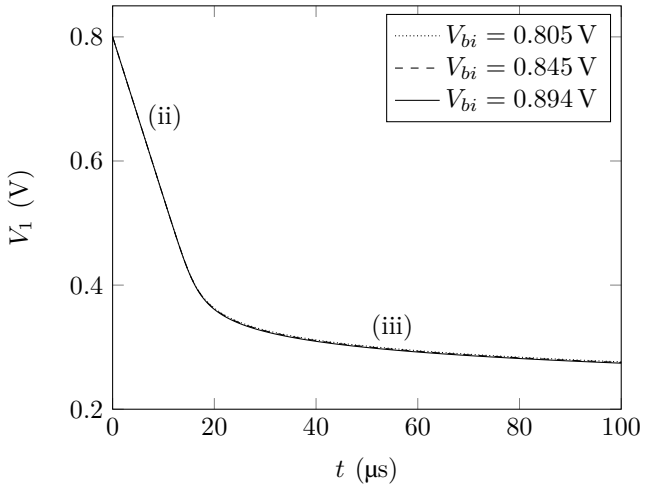


**Fig. 9**: Simulated OCVD signals for various built-in voltages $V_{bi}$

## 4 Results in silicon diode

This section is dedicated to the fitting procedure of an experimental OCVD signal for a silicon diode (Vishay 1N4007). The aim is to validate the extraction of $\tau_{eff}$, $N_l$, $V_{bi}$ and $R_{sh}$ and so, to highlight the flexibility of OCVD method. We assumed the diode is an asymmetric junction. We decided first to apply our model to a silicon diode because this semiconductor has well know properties on the one hand, and it has a long lifetime that guarantees clear (ii) and (iii) regions on the other hand. Regarding the silicon diode, we have no information about its design (thickness layers, doping levels and so on). Thus we extracted the experimentally required variables from dark I-V and C-V curves in order to compare them to those obtained by OCVD modelling.

### 4.1 *Experimental details*

OCVD characterization was carried out using the "series circuit" presented Fig. 10. The OCVD bench is composed of a 1 A current/voltage source (Keithley 2400), a 2 GHz bandwidth oscilloscope (Tektronix TDS784D), an n-type enhancement MOSFET (Semelab D2081UK) and a function generator (MB Electronique Wavetek FG3B) to drive the MOSFET. The MOSFET has been selected for its low commutation time ($< 30$ ns). As the design of the silicon diode (Vishay 1N4007) is unknown, we recorded a dark I-V characteristic using the Keithley 2400 and a C-V characteristic using a C-V plotter (EG&G Model 410) at 1 MHz. The dark I-V curve allows to determine the ideality factor and the shunt resistance $R_{sh}$ while the C-V curve allows to extract $N_l$ and $V_{bi}$ from an asymmetric p-n junction [2, 27]. Both curves are presented in Fig. 11. The ideality factor has

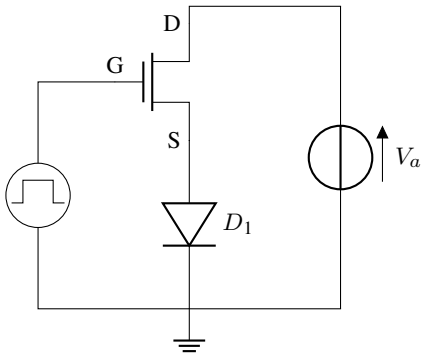


**Fig. 10**: OCVD "series" circuit used for silicon diode characterization.

been calculated through the local ideality factor $\eta(V)$ [28] with the following equation:

$$\eta(V) = \frac{q}{k_B T} \frac{\mathrm{d}V}{\mathrm{d}\,(\ln I)} \tag{13}$$

where $\mathrm{d}V/\mathrm{d}(\ln I)$ is the slope of the ln(I)-V curve at a given voltage represented Fig. 11. Then we obtained $\eta = 1.56$ by considering the average over the voltage range [0.2: 0.7 V]. The corresponding value of $\eta$ is represented in Fig. 11. We found $R_{sh} = 1.57 \times 10^6\,\Omega\,\mathrm{cm}^2$ (i.e. $R_{sh} = 5 \times 10^7\,\Omega$) considering the voltage range [−0.6: 0 V] on the dark I-V curve. Regarding the C-V curve, diffusion and SCR

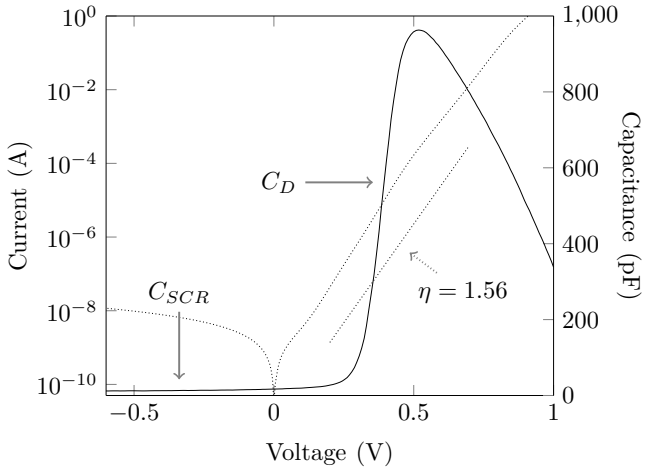


**Fig. 11**: Dark I-V and C-V characteristics of the silicon diode (Vishay 1N4007).

capacitances are clearly distinguishable and similar to those obtained from theory presented in Fig. 5. It is possible to extract $N_l$ and $V_{bi}$ by fitting the C-V curve with linear regression of $1/C_{SCR}^2$ [2, 27] given by:

$$\frac{1}{C_{SCR}^2} = -\frac{2V}{q\epsilon N_l A^2} + \frac{2V_{bi}}{q\epsilon N_l A^2} \tag{14}$$

where $A$ is the area of the silicon diode in $\mathrm{cm}^2$. Fig. 12 shows results of $1/C^2$ and its linear regression over the range [−0.7: 0 V]. We obtained $N_l = 2.19 \times 10^{12}\,\mathrm{cm}^{-3}$ and $V_{bi} = 0.694\,\mathrm{V}$ for a diode area of $3.14\,\mathrm{mm}^2$. All extracted parameters have been reported in Table 5.

As we didn't have any information about the nature of the junction, we performed modelling on the p-n$^+$ junction and the n-p$^+$ junction. We determined diffusion coefficient $D$ through (11) and calculated mobility $\mu_M$ from (12) for each junction assumption. We considered

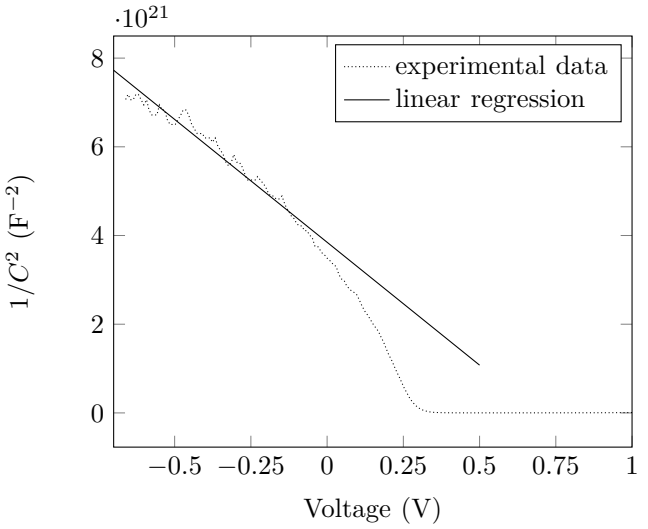


**Fig. 12**: Squared inverse SCR capacitance of the silicon diode (Vishay 1N4007) over the voltage.

**Table 5** Extracted parameters of the silicon diode (Vishay 1N4007) from dark I-V ($\eta$ and $R_{sh}$) and C-V ($N_l$ and $V_{bi}$) characteristics.

| $\eta$ [−] | $R_{sh}$ [$\Omega\,\mathrm{cm}^2$] | $N_l$ [$\mathrm{cm}^{-3}$] | $V_{bi}$ [V] |
|---|---|---|---|
| 1.56 | $1.57 \times 10^6$ | $2.19 \times 10^{12}$ | 0.694 |

electrons (holes) mobility for a p-n$^+$ junction (n-p$^+$ junction). This feature of charge carriers in semiconductors opens the possibility for our model to identify the junction type (p-n$^+$ ou n-p$^+$). But it also leads to a lack of accuracy if we do not choose the right junction type.

### 4.2 *Fitting process details*

The main purpose of our model is to extract various parameters such as $\tau_{eff}$, $N_l$, $V_{bi}$ and $R_{sh}$ from an experimental curve. This would make the OCVD a flexible method of measurement for semiconductors. Therefore, the model requires an optimization algorithm to properly fit the experimental curve where fitting variables would be $\tau_{eff}$, $N_l$, $V_{bi}$ and $R_{sh}$. We used an iterative optimization algorithm to minimize the following RMSE equation:

$$RMSE = \sqrt{\frac{1}{n}\sum_{i=1}^{n}\Big(V_{mod}(t_i) - V_{exp}(t_i)\Big)^2} \tag{15}$$

where $n$ is the number of measurements of the simulated signal, $V_{exp}(t_i)$ the experimental OCVD voltage at time $t_i$ and $V_{mod}(t_i)$ the simulated OCVD voltage at time $t_i$. OCVD voltage corresponds to $V_1$ in Fig. 2. RMSE is the Root Mean Square Error between $V_{exp}$ and $V_{mod}$ over the entire time range. The optimization algorithm we used is provided by Python-SciPy library called "scipy.optimize" with the function "minimize" [29]. We selected "Nelder-Mead" algorithm [30] which is the default one. We didn't work on algorithms during this work. Only 3 fitting variables were given to the algorithm for each simulation.

### 4.3 *Extraction results*

Presented below is an extraction of variables $R_{sh}$, $\tau_{eff}$, $N_l$ and $V_{bi}$ thanks to OCVD modelling. We compared these values obtained to those derived from the dark I-V and C-V characteristics. These values were taken as reference for comparison and are given in Tables 5 and 6. Lifetime is estimated from OCVD region (ii) which is linear and long enough to consider reliability of region (ii) by using (1). We present plots for a p-n$^+$ junction only (see Fig. 13 and Fig. 14)

**Table 6** Extracted parameters of the silicon diode (Vishay 1N4007) from OCVD fitting and I-V/C-V characteristics.

| | dark I-V and C-V | $Si_1$ | | $Si_2$ | |
|---|---|---|---|---|---|
| | | p-$n^+$ | n-$p^+$ | p-$n^+$ | n-$p^+$ |
| $RMSE$ [%] | - | 0.715 | | 0.569 | |
| $\tau_{eff}$ [µs] | - | $8.93^{\#}$ | | $8.78^{*}$ | |
| $N_l$ [$cm^{-3}$] | $2.19 \times 10^{12}$ | $5.76 \times 10^{11\#}$ | $4.11 \times 10^{11\#}$ | $9.11 \times 10^{11*}$ | $6.51 \times 10^{11*}$ |
| $V_{bi}$ [V] | 0.694 | $1.159^{\#}$ | | 0.694 | |
| $R_{sh}$ [$\Omega\,cm^2$] | $1.57 \times 10^6$ | $1 \times 10^9$ | | $3.58 \times 10^{5*}$ | $4.24 \times 10^{5*}$ |
| $\eta$ [−] | 1.56 | 1.56 | | 1.56 | |
| n [−] | - | 20 000 | | 20 000 | |
| Figure | | Fig. 13 | | Fig. 14 | |

$^{\#}$ fitting variables with random and consistent initial values of variables
$^{*}$ fitting variables with $Si_1$ results as initial values of variables

because the simulated signals are about the same for both p-$n^+$ and n-$p^+$ junctions.

First, we show results on Fig. 13 where $\tau_{eff}$, $N_l$ and $V_{bi}$ are the fitting variables while $R_{sh}$ is kept constant. We took a large value of the shunt resistance ($R_{sh} = 1 \times 10^9\,\Omega\,cm^2$) in order to avoid its influence on OCVD signal. Initial values of variables were selected arbitrary but are consistent for silicon diodes: $\tau_{eff} = 7\,\mu s$, $N_l = 1 \times 10^{15}\,cm^{-3}$ and $V_{bi} = 0.75\,V$.

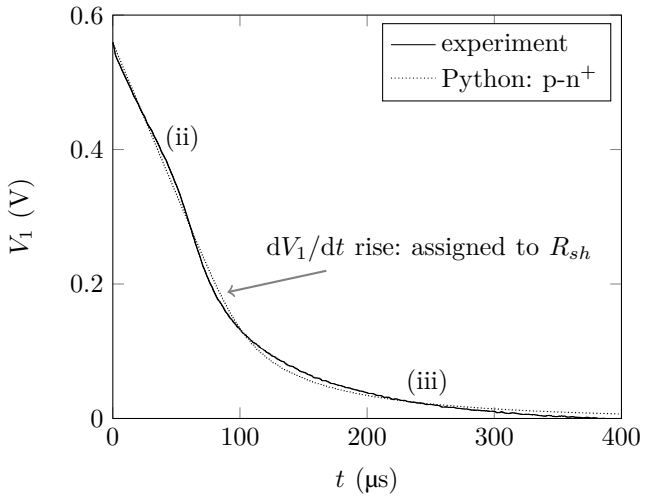


**Fig. 13**: OCVD signal: experiment and modelling. Modelling signal has been obtained with $\tau_{eff}$, $N_l$ and $V_{bi}$ as fitting variables.

We obtained $RMSE = 0.715\,\%$ (the same for a n-$p^+$ junction). However there are differences concerning the extracted variables depending on the junction type. Indeed, column $Si_1$ of Table 6 shows that the extracted values of $N_l$ are slightly different for the two kinds of junction while $\tau_{eff}$ are the same. It means, $\tau_{eff}$ does not depend on the junction type. $N_l$ and $\tau_{eff}$ values are consistent (around $5 \times 10^{11}\,cm^{-3}$ and 9 µs respectively) while $V_{bi}$ is far too high (1.16 V). Actually, it can not exceed 0.738 V that is obtained from (4) for $N_l = 5 \times 10^{11}\,cm^{-3}$ and $N_h = 5 \times 10^{20}\,cm^{-3}$ (roughly the intrinsic limit before being an alloy). We knew that the extraction of $V_{bi}$ would be difficult due to its low influence on OCVD signal (see subsection 3.3.4). Finally, it is not possible to conclude on the junction type even if $N_l$ in the case of the p-$n^+$ junction is slightly closer from $N_l$ extracted by C-V.

We performed a new simulation in order to carry out a fit with a consistent value of $V_{bi}$. Therefore, we fixed $V_{bi} = 0.694\,V$ (value extracted by C-V). The three fitting variables were $R_{sh}$, $N_l$ and $\tau_{eff}$. The initial values were those extracted previously (given in column $Si_1$ of Table 6). We chose $R_{sh}$ as a new fitting variable because the experimental OCVD signal shows a smooth increase of the slope in region (ii) around 0.35 V (see Fig. 13). As discussed previously, the increase of the decay rate can be explained by a shunt resistance effect (see subsection 3.3.3).

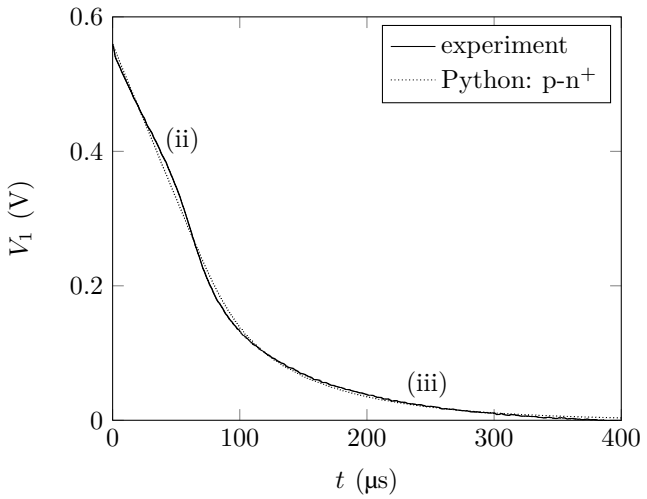


**Fig. 14**: OCVD signal: experiment and modelling. Modelling signal has been obtained with $\tau_{eff}$, $N_l$ and $R_{sh}$ as fitting variables.

The result for a p-$n^+$ junction is presented in Fig. 14. The use of $R_{sh}$ as new fitting variable does not enable to reduce drastically the RMSE whatever the junction type. The extracted variables are presented in column $Si_2$ of Table 6. Extracted lifetime $\tau_{eff}$ does not change notably by varying $R_{sh}$ instead of $V_{bi}$. Regarding $N_l$, the extraction provides results slightly higher than those obtained previously: $9.11 \times 10^{11}\,cm^{-3}$ and $6.51 \times 10^{11}\,cm^{-3}$ for a p-$n^+$ junction and an n-$p^+$ junction respectively. $R_{sh}$ values are also not so different for both types of junction. The n-$p^+$ junction presents the closest shunt resistance value ($4.24 \times 10^5\,\Omega\,cm^2$) from that obtained from the dark I-V curve ($1.57 \times 10^6\,\Omega\,cm^2$). Nevertheless, the junction type is also complicated to define. Thus, these results show how important it is to know the nature of the junction, otherwise, the reliability of the method could be affected. Moreover, many semiconductors such as III-V, show more imbalanced mobility (between electrons and holes) as compared to silicon [31]. That would probably lead to increase the gap in $N_l$ between both junction types.

The results of column $Si_2$ in Table 6 demonstrates that our model is able to properly fit the experimental OCVD curve of a silicon diode ($RMSE < 0.57\,\%$) and to extract rather suitable value of $R_{sh}$, $N_l$ and $\tau_{eff}$ with the support of a dark I-V curve (i.e. to determine $\eta$).

## 5 Conclusion and discussion

The theoretical OCVD signal presents a region with a linear decay which enables extraction of minority carrier effective lifetime $\tau_{eff}$ in

simple way. This region is often difficult to identify because of SCR capacitance and/or generation/recombination (G/R) current into the SCR. There is sometimes no linear region at all when lifetime is too short for instance. The quasi-steady stade mode [5] has been applied to the OCVD (know as "Suns-$V_{oc}$" [8]) in order to avoid detrimental SCR capacitance effect. Our approach has been to take advantage of this SCR capacitance effect since it also allows, theoretically, extraction of $N_l$, $V_{bi}$ and $R_{sh}$. Therefore, OCVD signal modelling is mandatory to overtake this difficulty. A first OCVD modelling has been carried out a few decades ago to explain influences of SCR capacitance and SCR G/R [7]. *M&B* did not derive $\tau_{eff}$ or other parameters from their modelling, although the OCVD signal is full of information.

We developed a model under Python programming language in order to simulate the OCVD signal. Our simulation is based on a lumped element model of one asymmetric diode in transient regime. We took *M&B* work as reference to develop our model. We went further by taking into account the dynamic of the SCR capacitance on the one hand and on the other hand, the joint influences of the SCR capacitance and the SCR G/R. We used this model to study the influences of $\tau_{eff}$, $N_l$, $R_{sh}$ and $V_{bi}$ on the OCVD signal. We first concluded that the lower $\tau_{eff}$ and the higher $N_l$, the lower the extraction accuracy. We also concluded that the low impact of $V_{bi}$ on OCVD signal makes its extraction unreliable.

Then OCVD signal fitting was carried out on an experimental curve of a silicon diode through an optimization algorithm provided by SciPy libraries. We reached $RMSE < 0.57\,\%$ for both junction types (n-p$^+$ and p-n$^+$). We have been able to extract a reliable value of $\tau_{eff}$ (i.e. no variation whatever is the junction type). We obtained values of $N_l$ and $R_{sh}$ rather close from those obtained from C-V and dark I-V characteristics. The extracted $N_l$ values are rather similar for both junction types with a constant ratio $N_{l(p-n^+)}/N_{l(n-p^+)} \approx 1.4$. This gap is probably due to the small difference between holes and electrons mobilities in silicon. However, this difference is usually higher in semiconductors such as III-V. It means this gap should be higher with III-V semiconductors impacting then the reliability of the extraction for unknown junction types. On the whole, the extracted values of $N_l$ and $R_{sh}$ were consistent but didn't allow to rule on the junction type.

We pointed out how important it is to know the right junction type in order to increase the reliability of $N_l$ and $R_{sh}$ extraction. By going further, this work could be complemented by assuming a symmetric junction through (3) or a different doping profile. Indeed, our model is based on the assumption of an abrupt junction. A non-abrupt junction would induce a different dynamics of the SCR capacitance over the time [32]. Then, the model could be improved by taking into account a second level of injection (two-diode model) in relevant case and different mobility models. Furthermore, it would be interesting to take into account the series resistance effect in order to simulate region (i). Finally, our model is only based on diode effects while it is clear that the MOSFET also affects the signal. Moreover, the circuit itself has different influences whether it is a "series" or "parallel" configuration. Finally, the method has been subjected to such a high lifetime junction which provides clear linear decay but this is not always the case. Therefore, today, we don't know if the flexibility of the method can be applied to OCVD signal having no linear decay but it opens the perspective to. We can clearly consider, the presented method is well suitable for Si solar cells since it has such a high lifetime, well known properties and an asymmetric design. However, its operation still has to be demonstrated for short lifetime junction whose clear linear decay is not guaranteed.

The first results presented here are promising and even open up the perspective for measuring short lifetime by OCVD with the support of a dark I-V curve and assuming a known design. Instead of measuring lifetime through the linear region (subjective method) it allows fast extraction by a fitting model (objective method). Since short lifetime usually does not provide linear region on OCVD signal, this work is of major importance to apply OCVD to semiconductors such as III-V. These materials are of major interest for PV applications such as multijunction solar cells. On the one hand, our approach makes the method less simple in terms of analysis, because semiconductor properties ($\mu$, $n_i$ and $\epsilon_r$) have to be known but it enhances greatly OCVD capabilities on the other hand. Furthermore, this is the first time, to the best of our knowledge, OCVD method demonstrates its measurement flexibility. It is a low-cost and a low-tech method so it represents an important breakthrough to achieve widespread use.

## Acknowledgments

Antoine Lemaire would like to thank Clément Lacroix, Hanany Tolba and Julien Nou for their support in Python programming and advices for the optimization algorithm. He is also grateful to Thomas Pettigrew.

## 6 References

1 A. Luque López and S. Hegedus, Eds., *Handbook of photovoltaic science and engineering*, 2nd ed., 2011.
2 D. K. Schroder, *Semiconductor material and device characterization*, 3rd ed., 2006.
3 ——, "Carrier lifetimes in silicon," *IEEE transactions on Electron Devices*, vol. 44, no. 1, pp. 160–170, 1997.
4 E. Yablonovitch and T. J. Gmitter, "A contactless minority lifetime probe of heterostructures, surfaces, interfaces and bulk wafers," *Solid-State Electronics*, vol. 35, no. 3, pp. 261–267, Mar. 1992. [Online]. Available: http://www.sciencedirect.com/science/article/pii/003811019290230A
5 R. A. Sinton, A. Cuevas, and M. Stuckings, "Quasi-steady-state photoconductance, a new method for solar cell material and device characterization," in *Photovoltaic Specialists Conference, 1996., Conference Record of the Twenty Fifth IEEE.* IEEE, 1996, pp. 457–460. [Online]. Available: http://ieeexplore.ieee.org/xpls/abs_all.jsp?arnumber=564042
6 R. K. Ahrenkiel, "Measurement of minority-carrier lifetime by time-resolved photoluminescence," *Solid-State Electronics*, vol. 35, no. 3, pp. 239–250, 1992.
7 J. E. Mahan and D. L. Barnes, "Depletion layer effects in the open-circuit-voltage-decay lifetime measurement," *Solid-State Electronics*, vol. 24, no. 10, pp. 989–994, 1981. [Online]. Available: http://www.sciencedirect.com/science/article/pii/0038110181901246
8 R. A. Sinton and A. Cuevas, "A QSS open circuit voltage method for solar cell characterization," in *European PV solar energy conference*, 2000. [Online]. Available: http://www.sintoninstruments.com/PDFs/sinton-epvsc16-pcd.pdf
9 B. R. Gossick, "On the Transient Behavior of Semiconductor Rectifiers," *Journal of Applied Physics*, vol. 26, no. 11, pp. 1356–1365, Nov. 1955. [Online]. Available: http://aip.scitation.org/doi/10.1063/1.1721908
10 S. R. Lederhandler and L. J. Giacoletto, "Measurement of minority carrier lifetime and surface effects in junction devices," *Proceedings of the IRE*, vol. 43, no. 4, pp. 477–483, 1955. [Online]. Available: http://ieeexplore.ieee.org/abstract/document/4055436/
11 J. E. Mahan, T. W. Ekstedt, R. I. Frank, and R. Kaplow, "Measurement of minority carrier lifetime in solar cells from photo-induced open-circuit voltage decay," *IEEE Transactions on Electron devices*, vol. 26, no. 5, pp. 733–739, 1979.
12 M. A. Green, "Minority carrier lifetimes using compensated differental open circuit voltage decay," *Solid-state electronics*, vol. 26, no. 11, pp. 1117–1122, 1983.
13 M. Caussanel, A. Canals, S. K. Dixit, M. J. Beck, A. D. Touboul, R. D. Schrimpf, D. M. Fleetwood, and S. T. Pantelides, "Doping-Type Dependence of Damage in Silicon Diodes Exposed to X-Ray, Proton, and $He^+$ Irradiations," *IEEE Transactions on Nuclear Science*, vol. 54, no. 6, pp. 1925–1930, Dec. 2007. [Online]. Available: http://ieeexplore.ieee.org/document/4395007/
14 S. Bellone and G. Licciardo, "An Analog Circuit for Accurate OCVD Measurements," *IEEE Transactions on Instrumentation and Measurement*, vol. 57, no. 6, pp. 1112–1117, Jun. 2008. [Online]. Available: http://ieeexplore.ieee.org/document/4450600/
15 A. Lemaire, "Mesure par OCVD de la durée de vie des porteurs minoritaires dans des jonctions en GaSb, en GaAs et en Si : simulations et expérimentations," Ph.D. dissertation, Université de Perpignan Via Domitia, Laboratoire PROMES-CNRS, rambla de la thermodynamique 66000 Perpignan, Nov. 2019.
16 M. P. Deshmukh, R. A. Kumar, and J. Nagaraju, "Measurement of solar cell ac parameters using the time domain technique," *Review of scientific instruments*, vol. 75, no. 8, pp. 2732–2735, 2004.
17 P. C. Ariel, M. A. Cappelletti, and E. L. P. y Blanca, "A computerized method for carrier lifetime measurement in PN junctions at high and low-level injection," in *2010 Argentine School of Micro-Nanoelectronics, Technology and Applications (EAMTA).* IEEE, 2010, pp. 87–93.
18 S. M. Sze and K. K. Ng, *Physics of semiconductor devices*, 3rd ed., 2007.
19 L. Castañer, E. Vilamajo, J. Llaberia, and J. Garrido, "Investigations of the OCVD transients in solar cells," *Journal of Physics D: applied Physics*, p. 10, 1981. [Online]. Available: http://iopscience.iop.org/article/10.1088/0022-3727/14/10/019/pdf
20 M. Ochoa, C. Algora, P. Espinet-González, and I. García, "3-D modeling of perimeter recombination in GaAs diodes and its influence on concentrator solar cells," *Solar Energy Materials and Solar Cells*, vol. 120, pp. 48–58, Jan. 2014. [Online]. Available: https://linkinghub.elsevier.com/retrieve/pii/S092702481300408X
21 P. Espinet-Gonzalez, I. Rey-Stolle, M. Ochoa, C. Algora, I. García, and E. Barrigón, "Analysis of perimeter recombination in the subcells of GaInP/GaAs/Ge triple-junction solar cells," *Progress in Photovoltaics: Research*

*and Applications*, vol. 23, no. 7, pp. 874–882, 2015. [Online]. Available: https://onlinelibrary.wiley.com/doi/abs/10.1002/pip.2501
22 Python, "Welcome to Python," 2019. [Online]. Available: https://www.python.org/
23 J.-P. Colinge and F. Van de Wiele, *Physique des dispositifs semi-conducteurs*, 1996.
24 SciPy, "minimize(method='TNC') — SciPy v1.3.0 Reference Guide," 2019. [Online]. Available: https://docs.SciPy.org/doc/SciPy/reference/optimize.minimize-tnc.html#optimize-minimize-tnc
25 ——, "scipy.integrate.LSODA — SciPy v1.3.0 Reference Guide," 2019. [Online]. Available: https://docs.SciPy.org/doc/SciPy/reference/generated/SciPy.integrate.LSODA.html#SciPy.integrate.LSODA
26 G. Masetti, M. Severi, and S. Solmi, "Modeling of carrier mobility against carrier concentration in arsenic-, phosphorus-, and boron-doped silicon," *IEEE Transactions on Electron Devices*, vol. 30, no. 7, pp. 764–769, Jul. 1983.
27 C. Van Opdorp, "Evaluation of doping profiles from capacitance measurements," *Solid-State Electronics*, vol. 11, no. 4, pp. 397–406, Apr. 1968. [Online]. Available: http://www.sciencedirect.com/science/article/pii/0038110168900208
28 K. R. McIntosh, "Lumps, Humps and Bumps: Three Detrimental Effects in the Current-Voltage Curve of Silicon Solar Cells," p. 190, 2001.
29 SciPy, "minimize(method='Nelder-Mead') — SciPy v1.3.0 Reference Guide," 2019. [Online]. Available: https://docs.SciPy.org/doc/SciPy/reference/optimize.minimize-neldermead.html
30 ——, "Scipy.integrate.odeint — SciPy v1.3.0 Reference Guide," 2019. [Online]. Available: https://docs.SciPy.org/doc/SciPy/reference/generated/SciPy.integrate.odeint.html
31 M. Levinshtein, S. Rumyantsev, and M. Shur, *Levinshtein M. Rumyantsev S. Shur M.-Handbook series on semiconductor parameters. Volume 1*, ser. Handbook series. World Scientific, 1996, vol. 1.
32 B. R. Chawla and H. K. Gummel, "Transition region capacitance of diffused p-n junctions," *IEEE Transactions on Electron Devices*, vol. 18, no. 3, pp. 178 – 195, 1971. [Online]. Available: https://ieeexplore.ieee.org/abstract/document/1476494